

SCIENTIFIC REPORTS



OPEN

Highly efficient and stable inverted perovskite solar cell employing PEDOT:GO composite layer as a hole transport layer

Jae Choul Yu¹, Ji A Hong¹, Eui Dae Jung¹, Da Bin Kim¹, Soo-Min Baek², Sukbin Lee¹, Shinuk Cho³, Sung Soo Park², Kyoung Jin Choi¹ & Myoung Hoon Song¹ 

The beneficial use of a hole transport layer (HTL) as a substitution for poly(3,4-ethylenedioxythiophene): polystyrene sulfonate (PEDOT:PSS) is regarded as one of the most important approaches for improving the stability and efficiency of inverted perovskite solar cells. Here, we demonstrate highly efficient and stable inverted perovskite solar cells by applying a GO-doped PEDOT:PSS (PEDOT:GO) film as an HTL. The high performance of this solar cell stems from the excellent optical and electrical properties of the PEDOT:GO film, including a higher electrical conductivity, a higher work function related to the reduced contact barrier between the perovskite layer and the PEDOT:GO layer, enhanced crystallinity of the perovskite crystal, and suppressed leakage current. Moreover, the device with the PEDOT:GO layer showed excellent long-term stability in ambient air conditions. Thus, the enhancement in the efficiency and the excellent stability of inverted perovskite solar cells are promising for the eventual commercialization of perovskite optoelectronic devices.

Organic-inorganic perovskite structures have been regarded as promising next-generation optoelectronic materials due to their superior optical and electrical properties, simple solution processing, and low cost^{1–5}. In particular, the power conversion efficiency (PCE) values of perovskite solar cells have increased over the past few years from 3.8% to more than 22%^{6–16}. Moreover, the external quantum efficiency (EQE) values of the perovskite light-emitting diodes (PeLEDs) also have increased to 9.3% for green emission and 11.7% for near-infrared emission^{17–23}.

The structure of perovskite devices is classified into conventional and inverted categories. Although conventional perovskite solar cells generally operate at high efficiencies, they are not suitable for flexible devices because they contain a metal oxide as an electron transport layer, which is rigid and requires high-temperature processing for good electrical properties^{12,13,16}. On the other hand, inverted perovskite solar cells consisting of ITO/poly(3,4-ethylenedioxythiophene):polystyrene sulfonate (PEDOT:PSS)/perovskite/PCBM/Ag where ITO is indium-tin-oxide and PCBM is the fullerene derivative phenyl-C61-butyric acid methyl ester, can be fabricated by simple, low-temperature (150 °C) processing methods^{24–27}. PEDOT:PSS is widely used as a hole transport layer (HTL) in organic and perovskite optoelectronic devices because it provides a smooth surface on the ITO electrode. However, the high acidity of the PEDOT:PSS solution corrodes the ITO electrode and perovskite, which limits the stability and performance of organic and perovskite optoelectronic devices^{28,29}. Moreover, the inverted perovskite solar cells based on PEDOT:PSS exhibit low open circuit voltage (V_{oc}) and short circuit current (J_{sc}). This electrical disadvantage is due to the larger energy barrier between the perovskite and PEDOT:PSS layers, which limits charge extraction, and the poor electron blocking ability necessary for suppressing leakage current³⁰. Therefore, researchers are investigating a variety of materials as replacements for PEDOT:PSS, including metal oxides and doped or solvent-treated PEDOT:PSS layers^{31–34}.

¹School of Materials Science Engineering and KIST-UNIST Ulsan center for Convergent Materials/Low Dimensional Carbon Center/Perovtronic Research Center, Ulsan National Institute of Science and Technology (UNIST), UNIST-gil 50, Ulsan, 44919, Republic of Korea. ²School of Materials Science and Engineering, Ulsan National Institute of Science and Technology (UNIST), UNIST-gil 50, Ulsan, 44919, Republic of Korea. ³Department of Physics and EHSRC, University of Ulsan, Ulsan, 44610, Republic of Korea. Correspondence and requests for materials should be addressed to M.H.S. (email: mhsong@unist.ac.kr)

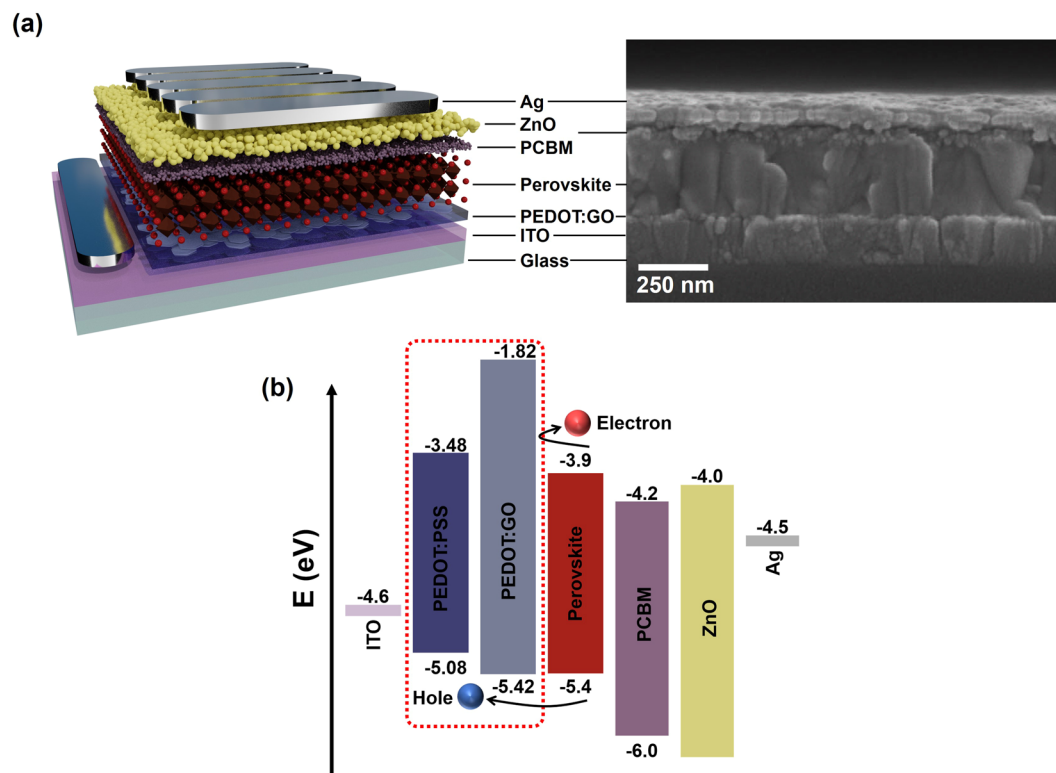


Figure 1. (a) The device schematic and SEM cross-sectional image of a perovskite solar cell (ITO/HTL/perovskite/PCBM/ZnO nanoparticles/Ag) and (b) relative energy levels of the various device components in the perovskite solar cells.

The metal oxides, such as nickel oxide (NiO_x) and Cu-doped nickel oxide (Cu:NiO_x), significantly enhance carrier mobility and air stability compared to PEDOT:PSS, resulting in the improvement of the device performance and long-term stability^{31,35,36}. Doped PEDOT:PSS exhibits better electrical conductivity and a lower highest occupied molecular orbital (HOMO) energy level, resulting in improvement of J_{sc} , V_{oc} and overall device performance³². Recently, Chen *et al.* have reported that the use of the solvent Dimethylformamide (DMF) to treat PEDOT:PSS improves device performance by enhancing electrical conductivity of PEDOT:PSS and reducing surface roughness³³. Unfortunately, these doped and solvent-treated PEDOT:PSS methods do not improve the device stability, which is why the stability still needs to be systemically studied.

In this work, we demonstrated highly efficient and stable perovskite solar cells by replacing the PEDOT:PSS with a PEDOT:PSS and a graphene oxide (PEDOT:GO) composite layer that acts as an HTL. The PEDOT:GO composite film exhibited a higher work function and better electrical conductivity compared to PEDOT:PSS. Moreover, the PEDOT:GO composite layer enhanced the crystallinity of the perovskite film and remarkably reduced leakage current in the perovskite solar cell. The optimized PEDOT:GO-based perovskite solar cell showed a significantly enhanced PCE of 18.09% with negligible J - V hysteresis. In addition, the encapsulated perovskite solar cell with the PEDOT:GO composite layer showed excellent long-term stability under ambient operating conditions.

Results

Figure 1(a) and (b) show the corresponding device schematic and cross-sectional scanning electron microscope (SEM) image and relative energy levels of components in the whole device consisting of ITO/HTL/perovskite/PCBM/ZnO nanoparticles/Ag, respectively. To understand how PEDOT:GO-based perovskite solar cells may improve efficiency and stability compared to PEDOT:PSS, we observed the structure and morphology of precursors and the final composite. The GO film prepared with pristine GO solution (Highly Concentrated Graphene Oxide, Graphene Supermarket) exhibited a very large and non-uniform GO flake size of about $10\ \mu\text{m}$, as shown in Fig. S1(a). To obtain a small and uniform size of GO flakes, the pristine GO solution was ultrasonicated and the pH value was adjusted to pH 9. After 5 hours of sonication, a homogeneous dispersion of 500 nm sized GO flakes was obtained, as shown in Fig. S1(c). The sizes of GO flakes change with time of sonication. SEM images of the PEDOT:GO composite film fabricated with these homogeneous GO flakes (5 hours of sonication) showed a similar morphology to pristine PEDOT:PSS films, whereas the PEDOT:GO composite film with non-uniform and large GO flakes (without and with sonication for 0.5 h) showed a significantly rougher surface, as shown in Fig. S2.

To further analyze the morphology of perovskite film further, the perovskite film prepared on pristine PEDOT:PSS and PEDOT:GO composite films (with various flake sizes of GO) were observed using atomic force

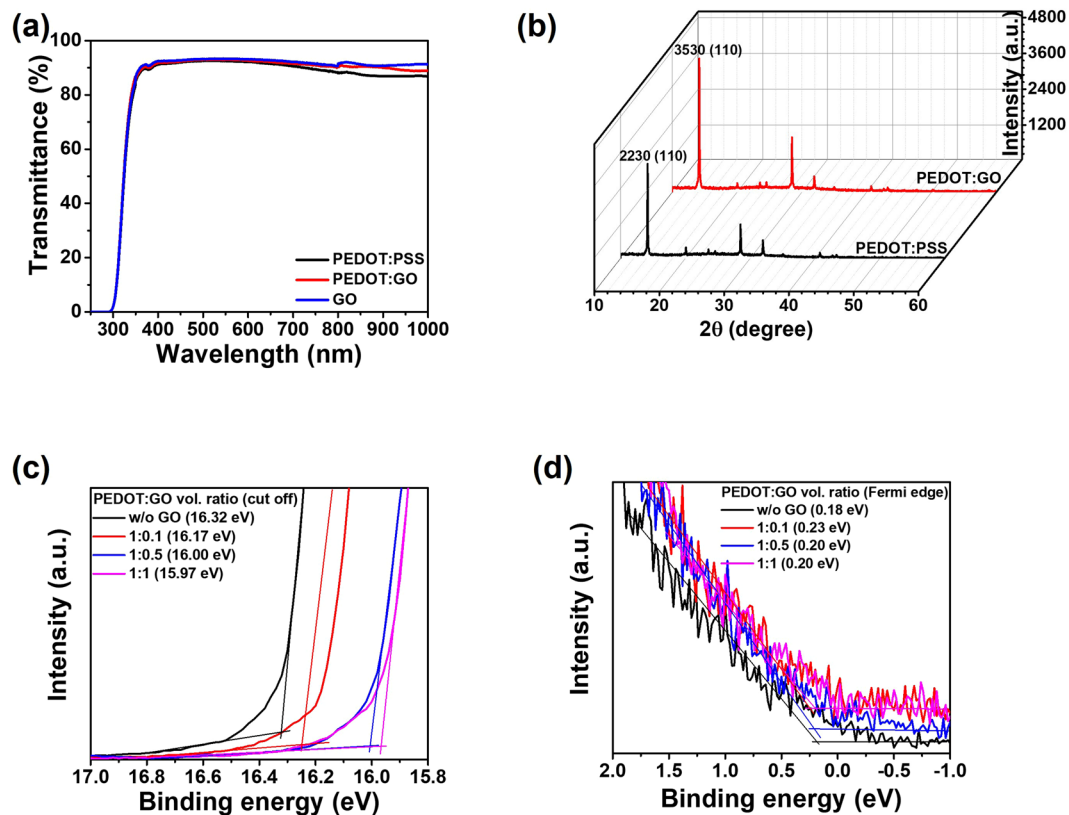


Figure 2. (a) Transmittance spectra of PEDOT:PSS, PEDOT:GO composite, and GO, (b) XRD patterns of perovskite prepared on PEDOT:PSS and PEDOT:GO composite films with preferred orientation along the (110) directions. The UPS measurements of PEDOT:PSS and PEDOT:GO composite (vol. ratio of 1:0.1, 1:0.5, and 1:1) films; (c) secondary electron cutoff regions and (d) Fermi edge (valence band edge) regions, respectively.

microscopy (AFM), as shown in Fig. S3. The perovskite films deposited onto PEDOT:GO composite layers (where GO was sonicated for 5 h) and pristine PEDOT:PSS showed a similar morphology, with low root-mean-square (RMS) roughness values of 16.0 and 15.2 nm, respectively. However, the perovskite films prepared on PEDOT:GO composite layers (without and with sonication for 0.5 h) exhibited a significantly rougher surface with high RMS roughness values of 23.4 and 18.8 nm, respectively.

To investigate the effect of a PEDOT:GO composite layer on perovskite films and devices, the transmittance of the PEDOT:GO composite film was measured and correlated to the crystallinity. Since sunlight reaches the perovskite layer after passing through its HTL, high optical transparency of an HTL is necessary for efficient light harvesting and improved absorbance of the perovskite film. To confirm the transparency of HTLs, the transmittance spectra of PEDOT:PSS, PEDOT:GO composite (vol. ratio of 1:0.5), and GO films all with film thicknesses of 30 nm were measured, as shown in Fig. 2(a). The GO film alone had the highest transparency above 700 nm, and the PEDOT:GO composite film showed higher transmittance above 700 nm than the pristine PEDOT:PSS film, attributed to the higher transparency of the GO film. In particular, the transmittance of the PEDOT:GO composite film between 800 and 1000 nm was excellent, which would be significant if used as an HTL for Si/perovskite tandem solar cells.

The crystallinity of the perovskite film prepared on pristine PEDOT:PSS and PEDOT:GO composite layers was confirmed by X-ray diffraction (XRD) spectra in Fig. 2(b). The peak at 14.10° corresponds to the (110) orientation of the perovskite film, and the peak intensity of that orientation for the PEDOT:GO composite (vol. ratio of 1:0.5) was 160% of that for the pristine PEDOT:PSS layer. It has been previously reported that the crystallinity of perovskite films prepared on a GO layer increases because perovskite crystals preferentially grow on the GO layer rather than the PEDOT:PSS film³⁷. Therefore, the enhancement of the crystallinity of the perovskite layer may originate from the presence of GO in the PEDOT:GO composite film. Structural changes that occur as a result of improved perovskite crystallinity on the PEDOT:GO composite film may also influence the device efficiency. The preferred orientation of (110) in perovskite films has been reported to increase the fill factor (FF) and V_{oc} in perovskite solar cells³⁸.

In addition, the work functions of the PEDOT:PSS and PEDOT:GO composites (vol. ratio of 1:0.1, 1:0.5 and 1:1) were measured using ultra-violet photoemission spectroscopy (UPS) to investigate the change of the work function due to the presence of GO in PEDOT:PSS. Figure 2(c) and (d) show the binding energy at secondary electron cut-off and Fermi-edge regions, respectively. The work functions of the PEDOT:PSS, PEDOT:GO composites (vol. ratio of 1:0.1, 1:0.5 and 1:1) were determined to be 4.90, 5.05, 5.22 and 5.25 eV, respectively. The highest occupied molecular orbital (HOMO) levels are calculated by the sum of the work functions and Fermi

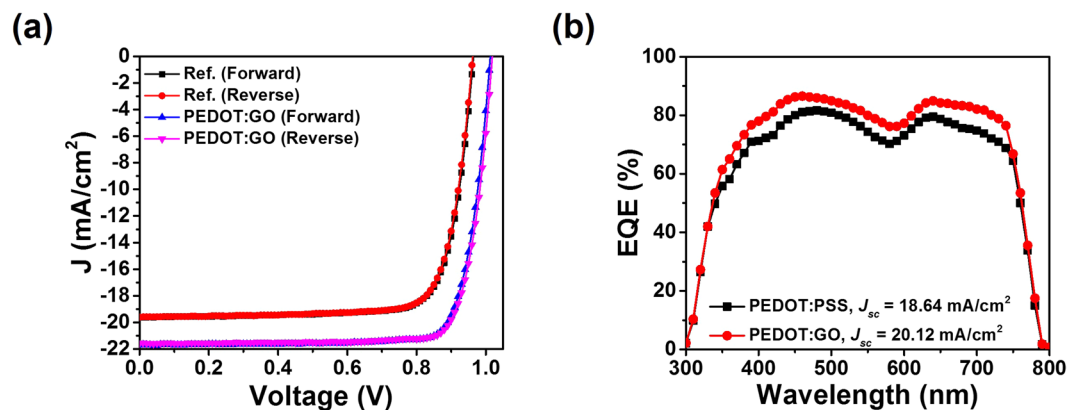


Figure 3. (a) J - V curves of the best-performing perovskite solar cells with PEDOT:PSS and a PEDOT:GO composite film under forward and reverse bias. (b) The external quantum efficiency (EQE) spectra of the best-performing cells.

edge energy³⁹. Therefore, the values of HOMO levels for the PEDOT:PSS and PEDOT:GO composite (vol. ratio of 1:0.1, 1:0.5 and 1:1) were determined to be 5.08, 5.28, 5.42 and 5.45 eV. Interestingly, the work function of PEDOT:GO increased from 4.90 eV to 5.25 eV depending on the vol. ratio of GO in PEDOT:PSS. In fact, the benzoid-quinoid transition of PEDOT structure after mixing the GO and PEDOT:PSS solution was observed because both the highly oxidized functional group and the sp^2 conjugation of GO bring about hydrogen bonding and π - π stacking in the previous study⁴⁰. A few reports have demonstrated that the work function of PEDOT:PSS increases when the structure of PEDOT changes from benzoid to quinoid^{41,42}. Therefore, the increase of work function of PEDOT:GO may originate from the benzoid-quinoid transition of PEDOT.

To confirm the correlation between improved transmittance, crystallinity, and efficiency of the perovskite on the PEDOT:GO composite film and performance of a device made with this composite, perovskite solar cells prepared on pristine PEDOT:PSS and PEDOT:GO composite films were fabricated. Unfortunately, the PEDOT:GO composite-based devices produced with the large GO particles showed lower power conversion efficiencies (PCEs) than the reference cell, as shown in Fig. S4. It is well-known that device performance deteriorates in perovskite-based optoelectronic devices when the morphology of the perovskite film is deficient^{9,43,44}. However, the PEDOT:GO composite device fabricated with fine, uniform GO particles (where GO was sonicated for 5 h) exhibited a PCE of 16.16%, higher than the reference cell at 13.59%. The detailed photovoltaic parameters are summarized in Table S1.

Particle size and uniformity of GO affected the PCE, and the concentration of GO in PEDOT:GO composite layer also affected device performance, as confirmed in Fig. S5. The J - V curves of perovskite solar cells with various volume ratios of GO in PEDOT:GO composite layers (with GO particle sonication for 5 h) were determined. The device with PEDOT:GO composite layer (vol. ratio of 1:0.5) exhibited the highest PCE of 17.74%, with a higher J_{sc} , FF , and V_{oc} than other GO concentrations tested. However, an excessive amount of GO impaired device performance because the insulator property of GO reduces the charge extraction characteristics. The detailed photovoltaic parameters are summarized in Table S2.

The parameters of J_{sc} , FF , V_{oc} , and PCE were also measured to determine the quality of the device performance. Figure 3(a) and (b) show the J - V curves and EQE spectra of the best performing devices with PEDOT:GO and pristine PEDOT:PSS film as HTLs, respectively. The best performance of a perovskite solar cell with a PEDOT:GO composite layer corresponded to a J_{sc} of 21.55 mA/cm², an FF of 82.3%, a V_{oc} of 1.02 V, and a PCE of 18.09%. Weaker results were found for the best performing perovskite solar cell with a PEDOT:PSS film, where we found a J_{sc} of 19.61 mA/cm², an FF of 78.53%, a V_{oc} of 0.97 V, and a PCE of 14.95%, as shown in Fig. 3(a). A summary of the performance parameters for the best-performing solar cells is presented in Table 1. The perovskite solar cell with the optimized PEDOT:GO composite film exhibited higher EQE values in the overall range compared to the reference device, which supports the notion that the device with a PEDOT:GO composite layer facilitated efficient charge extraction and higher V_{oc} . In addition, both devices showed negligible J - V hysteresis. The steady-state photocurrent and output efficiency (SPO) was measured at the 0.87 V, as shown in Fig. S6. The perovskite solar cell with PEDOT:GO composite film achieved a stabilized current density of 20.30 mAcm⁻² and a stabilized PCE of 17.68%. This result supports the negligible J - V hysteresis of the perovskite solar cell with PEDOT:GO composite film.

To further investigate the effect of a PEDOT:GO composite film on the performance of the perovskite solar cell, the charge carrier dynamics via a time-correlated single photon count (TCSPC) and electrochemical impedance spectroscopy (EIS) were measured. Figure 4(a) and (b) show steady-state and time-resolved photoluminescence (PL) spectra of perovskite layers prepared on a PEDOT:PSS film and a PEDOT:GO composite film (vol. ratio of 1:0.5), respectively. The PL intensity of the perovskite film prepared on the PEDOT:GO composite decreased about 97%, whereas the PL intensity of perovskite film prepared on PEDOT:PSS film decreased about 88%. Moreover, the exciton lifetime of the perovskite film prepared on a PEDOT:GO composite exhibited a remarkable decrease (3.48 ns) compared to the perovskite film prepared on PEDOT:PSS film (14.76 ns).

Devices configuration	J SC [mA/cm]	V OC [V]	FF [%]	η [%]
ITO/PEDOT:PSS/perovskite/PCBM/ZnO NPs/Ag (Forward)	19.61	0.97	78.41	14.91
ITO/PEDOT:PSS/perovskite/PCBM/ZnO NPs/Ag (Reverse)	19.63	0.97	78.53	14.95
ITO/PEDOT:GO/perovskite/PCBM/ZnO NPs/Ag (Forward)	21.55	1.02	81.2	17.96
ITO/PEDOT:GO/perovskite/PCBM/ZnO NPs/Ag (Reverse)	21.55	1.02	82.3	18.09

Table 1. Summary of the device performance of perovskite solar cells with PEDOT:PSS and PEDOT:GO composite film under forward and reverse bias.

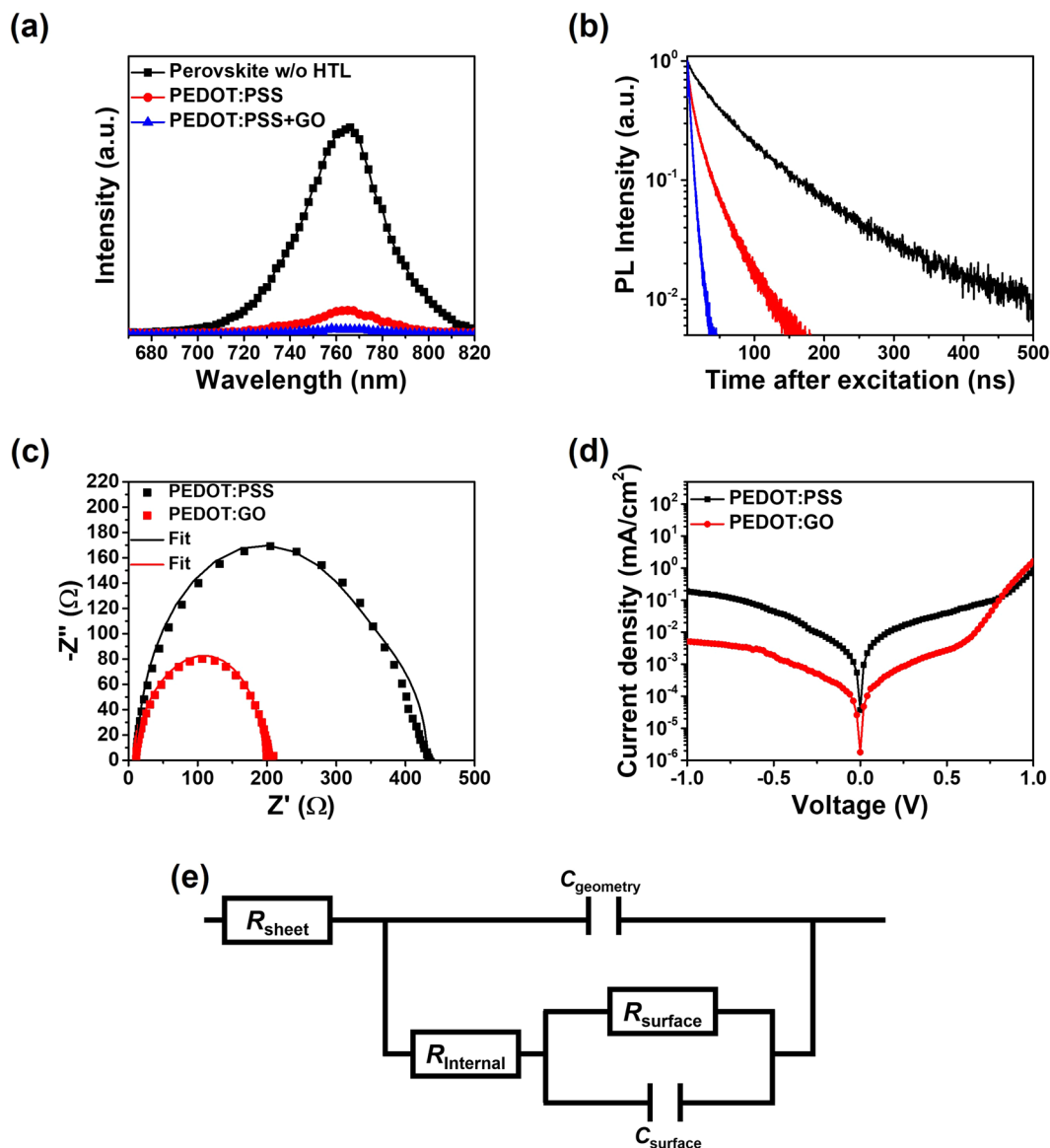


Figure 4. (a) Steady-state PL spectra and (b) time-resolved PL spectra of perovskite films prepared on PEDOT:PSS and PEDOT:GO composites, respectively. (c) Nyquist plots of perovskite solar cells with PEDOT:PSS and PEDOT:GO composite films. (d) Logarithmic plot of j - V characteristics of perovskite solar cells measured under the dark. (e) The equivalent circuit model for solar cells.

Consequently, the PL intensity and exciton lifetime of the perovskite film prepared on PEDOT:GO composite film showed a significant decrease compared to perovskite films without an HTL (PEDOT:PSS) because of a quenching effect. Thus, these results support improved hole extraction toward the anode using a PEDOT:GO composite layer as a HTL in the perovskite solar cells³². The corresponding parameters describing exciton lifetimes are also summarized in Table S3.

We also conducted electrochemical impedance spectroscopy (EIS) measurements of our perovskite solar cells to investigate the inner series resistances, which consist of sheet resistance (R_{sheet}) of the electrodes, internal resistance (R_{internal}) of device and surface recombination resistance (R_{surface}) at the interface between the adjacent charge carrier layer and electrode. Figure 4(c) shows the Nyquist plots of the perovskite solar cells with the PEDOT:GO composite and the PEDOT:PSS films. The equivalent circuit used for these devices is shown in Fig. 4(e). The experiment data were well described by the equivalent circuit and the fitting parameters, as shown in Fig. 4(c) and Table S4, respectively. In particular, the R_{internal} values exhibited 357.8 and 133.7 Ω for perovskite solar cells with PEDOT:PSS and PEDOT:GO composite films as HTLs, respectively. The smaller R_{internal} of the perovskite solar cell with PEDOT:GO composite layer is attributed to an enhanced charge extraction through energy level matching between HTL and perovskite layer and the enhancement of conductivity of PEDOT:GO, resulting in improved device photocurrent as well as improved PCE. Moreover, the suppression of leakage current was confirmed by the J - V curves of perovskite solar cells under a dark condition, as shown in Fig. 4(d). The current density of the perovskite solar cell with the PEDOT:GO composite film under reverse bias was approximately two orders of magnitude lower than that of the device with a pristine PEDOT:PSS film. In addition, the different shape of J - V curves of perovskite solar cells with PEDOT:PSS and PEDOT:GO composite layer occurs at a positive bias because the charge injection of device with PEDOT:GO composite layer is more efficient than that with PEDOT:PSS by reducing the injection barrier between a HTL and perovskite layer. This result also supports the notion that the photo-generated charge carriers are effectively extracted through the device³³.

To investigate the improvement of hole extraction between the HTL and perovskite layer, the current densities of the hole-only devices (ITO/PEDOT:PSS and PEDOT:GO/perovskite/PCBM/ZnO/MoO₃/Au) were compared, as shown in Fig. S7. The current density of the hole-only device with PEDOT:GO composite film was much larger than that of the hole-only device with pristine PEDOT:PSS film. This result supports the conclusion that the hole extraction in the perovskite solar cell with PEDOT:GO composite film was enhanced due to the higher electrical conductivity of the PEDOT:GO composite film and smaller contact barrier between perovskite layer and the PEDOT:GO. The HTL prepared using the mixture of PEDOT:PSS and graphene oxide (GO) solution for a PEDOT:GO composite layer showed higher electrical conductivity than a PEDOT:PSS film due to the benzoid-quinoid transition, as shown in Table S5, which had also been confirmed in our previous study⁴⁰. Moreover, GO can block the electrons from the perovskite layer because of large band gap, which facilitates the suppression of leakage current, thereby resulting in enhanced device performance.

To confirm the long-term stability of perovskite solar cells, encapsulated devices with PEDOT:PSS and PEDOT:GO composite films were measured under an ambient air condition, as shown in Fig. 5. The PCE of the perovskite solar cell with the PEDOT:PSS film rapidly decreased to 10% of its initial value after 25 days, whereas the perovskite solar cell with the PEDOT:GO composite film maintained 80% of its initial PCE with a much slower degradation rate. The main reason for the PCE deterioration in PEDOT:PSS-based perovskite solar cells stems from the significant decrease of J_{sc} and FF , which is related to the degradation of ITO and the perovskite layer by highly acidic PEDOT:PSS. This phenomenon is similar to previous reports in the organic photovoltaic field^{45,46}. Thus, perovskite solar cell fabricated with a PEDOT:GO composite film was more stable than the reference cell because it reduced the degradation of ITO and perovskite layer by the low acidic property of the GO solution (pH 9). It has also been reported that avoiding acidic conditions when processing PEDOT:PSS or GO improves the long-term stability of perovskite solar cells^{47,48}.

To increase the statistical significance of our efficiency data, 50 samples of each PEDOT:PSS and PEDOT:GO composite film were fabricated and measured; histograms of J_{sc} , V_{oc} , FF , and PCE for both composites are presented in Fig. S8. The perovskite solar cells with PEDOT:GO composite films exhibited 17.6% higher PCE values and higher values of J_{sc} , V_{oc} , and FF compared with those with PEDOT:PSS film.

In addition, we fabricated perovskite light-emitting diodes (PeLEDs) to investigate the applicability of a PEDOT:GO composite layer in optoelectronic devices. Figure S9 shows characteristics of PeLEDs with PEDOT:PSS and optimized PEDOT:GO composite films, including the J - V curve, luminance vs. voltage (L - V), luminous efficiency vs. voltage, and EQE vs. voltage. The PeLED with the PEDOT:PSS film exhibited a maximum luminous efficiency of 3.14 cd/A and an EQE of 0.67%. On the other hand, the PeLED with an optimized PEDOT:GO composite layer exhibited a significantly enhanced maximum luminous efficiency of 10.70 cd/A and a EQE of 2.29%, which represents a significant enhancement of 340%. This enhanced efficiency originates from the improved electrical conductivity and the reduced contact barrier between the PEDOT:GO composite and perovskite films. This result clearly supports the conclusion that the use of a PEDOT:GO composite layer improves the efficiency of perovskite optoelectronic devices. The detailed device performance values of PeLEDs with PEDOT:PSS and PEDOT:GO composite films are summarized in Table S6.

Discussion

In summary, we demonstrated a simple method for obtaining highly efficient and stable inverted perovskite solar cells by introducing a PEDOT:GO composite film. The inverted perovskite solar cell with an optimized PEDOT:GO composite film showed a PCE of 18.09%, which is higher than that of the perovskite solar cell with a pristine PEDOT:PSS film (14.95%), and both devices had negligible J - V hysteresis. The high PCE of the perovskite solar cell originated from the superior properties of the PEDOT:GO composite film, including higher optical transmittance over 700 nm, higher electrical conductivity, higher work function to reduce the contact barrier between the perovskite layer and the PEDOT:GO layer, enhanced crystallinity of the perovskite crystal, and suppressed leakage current. These results improved charge carrier extraction and open circuit voltage in the device. In particular, the perovskite solar cell with the PEDOT:GO composite film produced highly enhanced long-term stability with 80% maintenance from its initial PCE after 25 days, while the perovskite solar cell with PEDOT:PSS film showed a decline in PCE. Therefore, we believe that this simple method for introducing

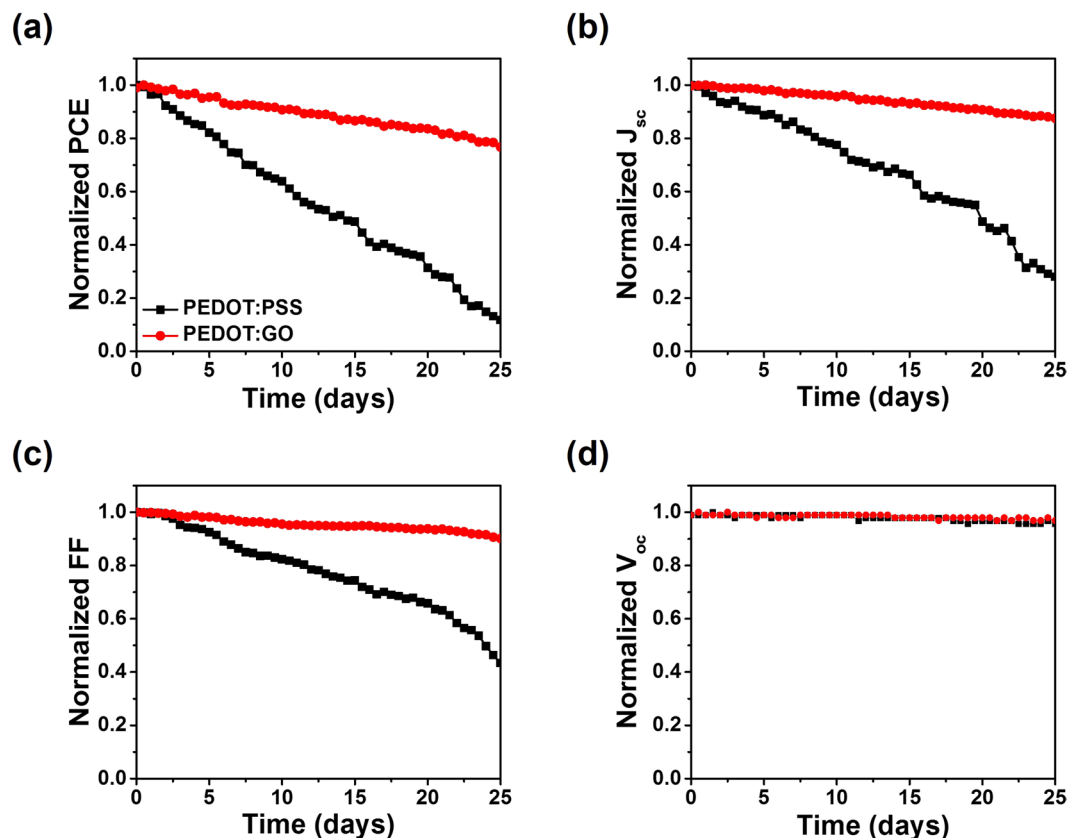


Figure 5. Stability characteristics of the perovskite solar cells with PEDOT:PSS and PEDOT:GO composite films under ambient air conditions: (a) Normalized PCE, (b) Normalized J_{sc} , (c) Normalized FF, and (d) Normalized V_{oc} , respectively.

PEDOT:GO composite film in perovskite solar cells improves efficiency and long-term stability and facilitates the commercialization of perovskite optoelectronic devices.

Methods

Materials. [6,6]-Phenyl-C71-butyric acid methyl ester (PCBM) was purchased from 1-Material. ZnO nanoparticle dispersed in IPA solution was purchased from Nanograde AG (Product No. N-10). The graphene oxide (GO) solution with concentration of 5 g/L in water was purchased from graphene supermarket (Product No. SKU-HCGO-W-175). All other materials were purchased according to the previous report⁴⁰.

Preparation of the PEDOT:GO composite solution. The GO solution was sonicated for various time (0–5 hrs), and then the PEDOT:GO solution was prepared according to the previous report⁴⁰.

Device fabrication. The configuration of perovskite solar cells was ITO/HTLs/perovskite/PCBM/ZnO nanoparticle/Ag. The HTLs such as PEDOT:PSS or PEDOT:GO composite were spin-coated onto the pre-patterned ITO substrate at 5,000 rpm for 45 s and annealed at 145 °C for 10 min. The substrates were then transferred into a glove box filled with pure N_2 . Then perovskite precursor solution (1.4 M PbI_2 , 1.33 M MAI and 0.07 M MABr in co-solvent of DMSO:GBL at vol ratio of 3:7) was spin-coated onto PEDOT:PSS and PEDOT:GO composite films via a consecutive 2-step method at 500 rpm and 5000 rpm for 5 and 25 s, respectively. During the spin-casting at 5,000 rpm, the chlorobenzene (300 μ L) was dropped onto the substrate and then annealed at 100 °C for 20 min. The PCBM solution dispersed in chlorobenzene (1.77 wt. %) and ZnO nanoparticle dispersion were sequentially spin-coated onto the perovskite layer at 2,000 rpm and 4,000 rpm for 45 s, respectively. The devices were completely fabricated by thermal deposition of 100 nm silver as a cathode under vacuum condition of $<2 \times 10^{-6}$ Torr. The devices area was 0.135 cm^2 defined by shadow mask.

Characterization of perovskite film and HTLs. The UPS spectra were measured using an ultra-high vacuum UPS system (ESCALAB 250Xi, Thermo Scientific) at 1×10^{-9} torr with a He (21.2 eV) ultraviolet source: all samples were biased at -5 V and were measured step size of 0.02 eV. The work function of HTLs (PEDOT:PSS, GO and PEDOT:GO) was calculated using the equation,

$$\Phi = P_{IN} - (E_{CE} - E_F) \quad (1)$$

where where Φ is the work function, P_{IN} is the incident photon energy (21.2 eV), E_{CE} is the binding energy at cut-off region and E_F is the binding energy at the Fermi level, which is zero, respectively. The HOMO level are calculated by the sum of the work functions and the Fermi edge energy³⁹.

To measure the conductivity of HTLs, 500 nm-thick PEDOT:GO and PEDOT:PSS films were prepared to obtain reliable conductivity values within limited resolution. The electric conductivity of PEDOT:GO and PEDOT:PSS films could be obtained by using 4-point probe measurement (CMT-SR2000N, Korea, measurement range: 1 m Ω /sq~2 M Ω /sq) and thickness measurements with a profilometer (KLA_Tencor, USA). Transmittance of PEDOT:PSS, PEDOT:GO and GO film were evaluated by UV-Vis-NIR spectrophotometer (Agilent Tec., Cary 5000). The impedance spectroscopy was performed using a potentiostat (Gamry Instruments, Reference 600TM) at 0.7 V. The oscillating voltage was 10 mV and the frequencies were ranged from 1 MHz to 1 Hz.

References

- D'Innocenzo, V. *et al.* Excitons versus free charges in organo-lead tri-halide perovskites. *Nature Communications* **5**, 3586, <https://doi.org/10.1038/ncomms4586> (2013).
- Stranks, S. D. *et al.* Electron-Hole Diffusion Lengths Exceeding 1 Micrometer in an Organometal Trihalide Perovskite Absorber. *Science* **342**, 341–344, <https://doi.org/10.1126/science.1243982> (2013).
- Xing, G. *et al.* Long-Range Balanced Electron- and Hole-Transport Lengths in Organic-Inorganic CH₃NH₃PbI₃. *Science* **342**, 344–347, <https://doi.org/10.1126/science.1243167> (2013).
- Wehrenfennig, C., Eperon, G. E., Johnston, M. B. & Snaith, H. J. & Herz, L. M. High Charge Carrier Mobilities and Lifetimes in Organolead Trihalide Perovskites. *Advanced Materials* **26**, 1584–1589, <https://doi.org/10.1002/adma.201305172> (2014).
- Green, M. A., Ho-Baillie, A. & Snaith, H. J. The emergence of perovskite solar cells. *Nat Photon* **8**, 506–514, <https://doi.org/10.1038/nphoton.2014.134> (2014).
- Kojima, A., Teshima, K., Shirai, Y. & Miyasaka, T. Organometal Halide Perovskites as Visible-Light Sensitizers for Photovoltaic Cells. *Journal of the American Chemical Society* **131**, 6050–6051, <https://doi.org/10.1021/ja809598r> (2009).
- Im, J.-H., Lee, C.-R., Lee, J.-W., Park, S.-W. & Park, N.-G. 6.5% efficient perovskite quantum-dot-sensitized solar cell. *Nanoscale* **3**, 4088–4093, <https://doi.org/10.1039/C1NR10867K> (2011).
- Lim, K.-G. *et al.* Boosting the Power Conversion Efficiency of Perovskite Solar Cells Using Self-Organized Polymeric Hole Extraction Layers with High Work Function. *Advanced Materials* **26**, 6461–6466, <https://doi.org/10.1002/adma.201401775> (2014).
- Yu, J. C. *et al.* High-Performance Planar Perovskite Optoelectronic Devices: A Morphological and Interfacial Control by Polar Solvent Treatment. *Advanced Materials* **27**, 3492–3500, <https://doi.org/10.1002/adma.201500465> (2015).
- Burschka, J. *et al.* Sequential deposition as a route to high-performance perovskite-sensitized solar cells. *Nature* **499**, 316–319, <https://doi.org/10.1038/nature12340> (2013).
- Zhou, H. *et al.* Interface engineering of highly efficient perovskite solar cells. *Science* **345**, 542–546, <https://doi.org/10.1126/science.1254050> (2014).
- Jeon, N. J. *et al.* Compositional engineering of perovskite materials for high-performance solar cells. *Nature* **517**, 476–480, <https://doi.org/10.1038/nature14133> (2015).
- Yang, W. S. *et al.* High-performance photovoltaic perovskite layers fabricated through intramolecular exchange. *Science* **348**, 1234–1237, <https://doi.org/10.1126/science.aaa9272> (2015).
- Chen, W. *et al.* Efficient and stable large-area perovskite solar cells with inorganic charge extraction layers. *Science* **350**, 944–948, <https://doi.org/10.1126/science.aad1015> (2015).
- Bi, D. *et al.* Polymer-templated nucleation and crystal growth of perovskite films for solar cells with efficiency greater than 21%. *Nature Energy* **1**, 16142, <https://doi.org/10.1038/nenergy.2016.142> (2016).
- Yang, W. S. *et al.* Iodide management in formamidinium-lead-halide-based perovskite layers for efficient solar cells. *Science* **356**, 1376–1379, <https://doi.org/10.1126/science.aan2301> (2017).
- Tan, Z.-K. *et al.* Bright light-emitting diodes based on organometal halide perovskite. *Nat Nano* **9**, 687–692, <https://doi.org/10.1038/nnano.2014.149> (2014).
- Kim, Y.-H. *et al.* Multicolored Organic/Inorganic Hybrid Perovskite Light-Emitting Diodes. *Advanced Materials* **27**, 1248–1254, <https://doi.org/10.1002/adma.201403751> (2015).
- Yu, J. C. *et al.* Improving the Stability and Performance of Perovskite Light-Emitting Diodes by Thermal Annealing Treatment. *Advanced Materials* **28**, 6906–6913, <https://doi.org/10.1002/adma.201601105> (2016).
- Cho, H. *et al.* Overcoming the electroluminescence efficiency limitations of perovskite light-emitting diodes. *Science* **350**, 1222–1225, <https://doi.org/10.1126/science.aad1818> (2015).
- Yuan, M. *et al.* Perovskite energy funnels for efficient light-emitting diodes. *Nat Nano* **11**, 872–877, <https://doi.org/10.1038/nnano.2016.110> (2016).
- Wang, N. *et al.* Perovskite light-emitting diodes based on solution-processed self-organized multiple quantum wells. *Nat Photon* **10**, 699–704, <https://doi.org/10.1038/nphoton.2016.185> (2016).
- Xiao, Z. *et al.* Efficient perovskite light-emitting diodes featuring nanometre-sized crystallites. *Nat Photon* **11**, 108–115, <https://doi.org/10.1038/nphoton.2016.269> (2017).
- Jeng, J.-Y. *et al.* CH₃NH₃PbI₃ Perovskite/Fullerene Planar-Heterojunction Hybrid Solar Cells. *Advanced Materials* **25**, 3727–3732, <https://doi.org/10.1002/adma.201301327> (2013).
- You, J. *et al.* Low-Temperature Solution-Processed Perovskite Solar Cells with High Efficiency and Flexibility. *ACS Nano* **8**, 1674–1680, <https://doi.org/10.1021/nn406020d> (2014).
- Shao, Y., Yuan, Y. & Huang, J. Correlation of energy disorder and open-circuit voltage in hybrid perovskite solar cells. *Nature Energy* **1**, 15001, <https://doi.org/10.1038/nenergy.2015.1> (2016).
- Nie, W. *et al.* High-efficiency solution-processed perovskite solar cells with millimeter-scale grains. *Science* **347**, 522–525, <https://doi.org/10.1126/science.aaa0472> (2015).
- Hou, F. *et al.* Efficient and stable planar heterojunction perovskite solar cells with an MoO₃/PEDOT:PSS hole transporting layer. *Nanoscale* **7**, 9427–9432, <https://doi.org/10.1039/C5NR01864A> (2015).
- Kim, D. B. *et al.* Improved performance of perovskite light-emitting diodes using a PEDOT:PSS and MoO₃ composite layer. *Journal of Materials Chemistry C* **4**, 8161–8165, <https://doi.org/10.1039/C6TC02099B> (2016).
- Chang, S. H. *et al.* Improving the efficiency of CH₃NH₃PbI₃ based photovoltaics by tuning the work function of the PEDOT:PSS hole transport layer. *Solar Energy* **122**, 892–899, <https://doi.org/10.1016/j.solener.2015.10.018> (2015).
- Jeng, J.-Y. *et al.* Nickel Oxide Electrode Interlayer in CH₃NH₃PbI₃ Perovskite/PCBM Planar-Heterojunction Hybrid Solar Cells. *Advanced Materials* **26**, 4107–4113, <https://doi.org/10.1002/adma.201306217> (2014).
- Liu, D. *et al.* Improved performance of inverted planar perovskite solar cells with F4-TCNQ doped PEDOT:PSS hole transport layers. *Journal of Materials Chemistry A* **5**, 5701–5708, <https://doi.org/10.1039/C6TA10212C> (2017).
- Chen, K. *et al.* Charge-Carrier Balance for Highly Efficient Inverted Planar Heterojunction Perovskite Solar Cells. *Advanced Materials* **28**, 10718–10724, <https://doi.org/10.1002/adma.201604048> (2016).

34. Zuo, C. & Ding, L. Modified PEDOT Layer Makes a 1.52 V Voc for Perovskite/PCBM Solar Cells. *Advanced Energy Materials* **7**, 1601193, <https://doi.org/10.1002/aenm.201601193> (2017).
35. You, J. *et al.* Improved air stability of perovskite solar cells via solution-processed metal oxide transport layers. *Nat Nano* **11**, 75–81, <https://doi.org/10.1038/nnano.2015.230> (2016).
36. Jung, J. W., Chueh, C.-C. & Jen, A. K. Y. A Low-Temperature, Solution-Processable, Cu-Doped Nickel Oxide Hole-Transporting Layer via the Combustion Method for High-Performance Thin-Film Perovskite Solar Cells. *Advanced Materials* **27**, 7874–7880, <https://doi.org/10.1002/adma.201503298> (2015).
37. Wu, Z. *et al.* Efficient planar heterojunction perovskite solar cells employing graphene oxide as hole conductor. *Nanoscale* **6**, 10505–10510, <https://doi.org/10.1039/C4NR03181D> (2014).
38. Song, D. *et al.* Dual function interfacial layer for highly efficient and stable lead halide perovskite solar cells. *Journal of Materials Chemistry A* **4**, 6091–6097, <https://doi.org/10.1039/C6TA00577B> (2016).
39. Kim, J., Park, H. J., Grigoropoulos, C. P., Lee, D. & Jang, J. Solution-processed nickel oxide nanoparticles with NiOOH for hole injection layers of high-efficiency organic light-emitting diodes. *Nanoscale* **8**, 17608–17615, <https://doi.org/10.1039/C6NR04643F> (2016).
40. Yu, J. C. *et al.* Highly Efficient Polymer-Based Optoelectronic Devices Using PEDOT:PSS and a GO Composite Layer as a Hole Transport Layer. *ACS Applied Materials & Interfaces* **6**, 2067–2073, <https://doi.org/10.1021/am4051487> (2014).
41. Lin, Y.-J. *et al.* Increasing the work function of poly(3,4-ethylenedioxythiophene) doped with poly(4-styrenesulfonate) by ultraviolet irradiation. *Applied Physics Letters* **91**, 092127, <https://doi.org/10.1063/1.2777147> (2007).
42. Yeo, J.-S. *et al.* Significant Vertical Phase Separation in Solvent-Vapor-Annealed Poly(3,4-ethylenedioxythiophene):Poly(styrene sulfonate) Composite Films Leading to Better Conductivity and Work Function for High-Performance Indium Tin Oxide-Free Optoelectronics. *ACS Applied Materials & Interfaces* **4**, 2551–2560, <https://doi.org/10.1021/am300231v> (2012).
43. Yu, J. C., Kim, D. B., Jung, E. D., Lee, B. R. & Song, M. H. High-performance perovskite light-emitting diodes via morphological control of perovskite films. *Nanoscale* **8**, 7036–7042, <https://doi.org/10.1039/C5NR05604G> (2016).
44. Yu, J. C. *et al.* Effect of the solvent used for fabrication of perovskite films by solvent dropping on performance of perovskite light-emitting diodes. *Nanoscale* **9**, 2088–2094, <https://doi.org/10.1039/C6NR08158D> (2017).
45. Meng, Y. *et al.* Improving the Stability of Bulk Heterojunction Solar Cells by Incorporating pH-Neutral PEDOT:PSS as the Hole Transport Layer. *ACS Applied Materials & Interfaces* **6**, 5122–5129, <https://doi.org/10.1021/am500336s> (2014).
46. Jørgensen, M., Norrman, K. & Krebs, F. C. Stability/degradation of polymer solar cells. *Solar Energy Materials and Solar Cells* **92**, 686–714, <https://doi.org/10.1016/j.solmat.2008.01.005> (2008).
47. Lee, D.-Y., Na, S.-I. & Kim, S.-S. Graphene oxide/PEDOT:PSS composite hole transport layer for efficient and stable planar heterojunction perovskite solar cells. *Nanoscale* **8**, 1513–1522, <https://doi.org/10.1039/C5NR05271H> (2016).
48. Wang, Q., Chueh, C.-C., Eslamian, M. & Jen, A. K. Y. Modulation of PEDOT:PSS pH for Efficient Inverted Perovskite Solar Cells with Reduced Potential Loss and Enhanced Stability. *ACS Applied Materials & Interfaces* **8**, 32068–32076, <https://doi.org/10.1021/acsami.6b11757> (2016).

Acknowledgements

This work was supported by the Korea Institute of Energy Technology Evaluation and Planning (KETEP) and the Ministry of Trade, Industry & Energy (MOTIE) of the Republic of Korea (No. 20163010012450). This work is financially supported by the KIST-UNIST partnership program (1.160097.01/2.160482.01) and Mid-Career Research Program (2015R1A2A2A01003263).

Author Contributions

J.C.Y. designed and conducted most of the experiments, analyzed the data and prepared the manuscript. J.A.H. and E.D.J. fabricated to make the perovskite solar cell. D.B. Kim performed the experimental TCSPC measurement. S.B. and S.S. Park performed the experimental impedance spectroscopy. S.C., S.L. and K.J.C. revised critically article. M.H.S. initiated the study, designed all the experiments, analyzed the data and prepared the manuscript. All authors discussed and commented on the manuscript.

Additional Information

Supplementary information accompanies this paper at <https://doi.org/10.1038/s41598-018-19612-7>.

Competing Interests: The authors declare that they have no competing interests.

Publisher's note: Springer Nature remains neutral with regard to jurisdictional claims in published maps and institutional affiliations.



Open Access This article is licensed under a Creative Commons Attribution 4.0 International License, which permits use, sharing, adaptation, distribution and reproduction in any medium or format, as long as you give appropriate credit to the original author(s) and the source, provide a link to the Creative Commons license, and indicate if changes were made. The images or other third party material in this article are included in the article's Creative Commons license, unless indicated otherwise in a credit line to the material. If material is not included in the article's Creative Commons license and your intended use is not permitted by statutory regulation or exceeds the permitted use, you will need to obtain permission directly from the copyright holder. To view a copy of this license, visit <http://creativecommons.org/licenses/by/4.0/>.

© The Author(s) 2018